# Thin glass shell oriented to Wide Field X-ray telescope

M. M. Civitani[a1], O. Citterio[a], S. Campana[a], P. Conconi[a], E. Mattaini[a,b], G. Pareschi[a], G. Tagliaferri[a], G. Parodi[c], V. Burwitz[d], G. D. Hartner[d], J. Arnold[e], S. Schuler[e], H. Combrinck[f], R. Freeman[f], R. Morton[f], P. Simpson[f], D. Walker[f]

[a]INAF-OAB Osservatorio Astronomico di Brera, Via E. Bianchi 46, 23807 Merate (LC), Italy
[b]INAF-IASF Milano, Via E. Bassini 15, 20133 Milano, Italy
[c]BCV Progetti, Via S. Orsola 1, 20123 Milano, Italy
[d]Max-Planck-Institut für extraterrestrische Physik (Germany)
[e]LT Ultra Precision Technology GmbH, Aftholderberg, Wiesenstrasse 9, 88634 Herdwangen-Schönach, Germany
[f]ZEEKO Ltd., Vulcan Way, Coalville, Leicestershire LE67 3FW, United Kingdom

## ABSTRACT

The next generation wide-field X-ray telescope (WFXT), to be implemented beyond eRosita and proposed within the NASA RFI call 2011, requires an angular resolution of less than 10 arcsec (with goal of 5") constant across a wide field of view (1 deg$^2$). To achieve this requirement the design is based on nested modified grazing incidence Wolter-I mirrors with polynomial profiles. Our goals in terms of mass and stiffness can be meet with the use of fused silica glass, a well-known material with good thermo-mechanical properties and polishability characteristics, together with an innovative polishing approach. Here we present the X-ray calibration results obtained for a prototypal shell tested in full-illumination mode at the Panter/MPE facility.

**Keywords:** X-ray Telescopes, Wide Field X-ray missions, X-ray calibrations, X-Ray shells, Deterministic polishing

## 1. INTRODUCTION

The Wide Field X-ray Telescope (WFXT) is a proposed medium-class mission dedicated to survey the sky in the soft X-ray band (0.2–7 keV; Murray et al. 2008). It foresees a X-ray telescope assembly whose main requirement is to be orders of magnitude more effective than previous and planned X-ray missions in carrying out surveys. This is obtained through a telescope design that makes use of polynomial profiles for the mirror shells, focal plane curvature and plate scale corrections (Burrows et al. 1992, Conconi et al. 2001, Conconi et al. 2010). In order to reach the effective area within the allocated mass, the shells need to be very thin, with wall thickness of few mm. Moreover, the shells are characterized by a very small Length-to-Diameter ratio (L/D), e.g. three times smaller than for XMM-Newton mirrors, making their fabrication more difficult. In the last years, a research activity has been carried out at the Osservatorio Astronomico di Brera (OAB) with the aim of defining a process for the realization of these glass shells with the direct polishing technique. Given that fused silica thermo-mechanical (T/M) properties (in particular low density and high Young modulus) are suitable to reach the necessary stiffness, tubes of fused silica, already available on the market, are used as raw material for the shell production. The deterministic direct polishing method is chosen to figure the shell to the needed accuracy: the technological challenge is to apply this method, already used for previous missions such as Einstein, Rosat, Chandra, to almost ten times thinner shells. To this aim, a temporary stiffening concept has been designed and realized.
A first prototypal shell, integrated in this stiffening structure, has undergone the out-of-roundness correction through fine grinding at Lt-Ultra and a first phase of polishing/superpolishing at Zeeko Ltd (Citterio et al. 2011). In the last months,

[1]marta.civitani@brera.inaf.it; phone +39 039 5971028; fax +39 039 5971001; www.brera.inaf.it

Space Telescopes and Instrumentation 2012: Ultraviolet to Gamma Ray,
edited by Tadayuki Takahashi, Stephen S. Murray, Jan-Willem A. den Herder,
Proc. of SPIE Vol. 8443, 84430Q · © 2012 SPIE · CCC code: 0277-786/12/$18 · doi: 10.1117/12.925906

the shell production has been completed in all the foreseen production steps. A preliminary X-ray calibration has been carried out in December 2011 at the Panter facility. In this paper we will review the shell development process and describe the calibration results. We also report the results of a measurement campaign aimed at understanding the possible influence of the dedicated jig to sustain the shell during the X-ray measurement. However, because the prototypal shell got broken during post-calibration activities, the latter results refer to a new integrated shell with the same geometry.

## 2. PROTOTYPAL SHELL#7 PRODUCTION

A first prototype shell (shell#7) has been manufactured to prove the feasibility of thin glass shell and to get a first assessment of the process. Its main geometric characteristics are summarized in Table 2-1.

**Table 2-1: Main characteristics of prototypal shell#7**

| Characteristic | Value |
|---|---|
| Focal length | 5500 mm |
| Diameter at intersection plane | 487 mm |
| Thickness | 2 mm |
| Total length | 200 mm |
| Material | Fused Silica |
| Mirror design | Polynomial |
| Weight | 1.368 kg |

The production flow (Citterio et al. 2011) that has been followed is summarized hereafter:

- Starting from a fused silica glass tube, the shell is firstly grinded with a double cone profile at the required thickness of a few millimeters. The raw fused silica tube and the first grinding operations have been provided by Heraeus Quarzglas GmbH & Co KG. (Figure 2-1-A)
- The shell is then characterized in terms of Out-Of-Roundness (OOR) errors, supporting it onto an astatic support jig (Figure 2-1-B). Afterwards the shell is integrated into a special "Shell Support Structure" (SSS), allowing us to perform the metrology, the machining and all the necessary steps up to the assembling into the final structure (Figure 2-1-C).
- By means of a fine grinding process on a high precision lathe, the OOR errors are corrected. These operations are performed by LT Ultra Precision Technology GmbH with grinding wheels and a metrological system that can be directly mounted on the lathe (Figure 2-2-A).
- The shell is figured and polished to the final polynomial profile, making use of a deterministic figuring method with a computer numerical control (CNC) polishing machine, that provides the corrective action according to the measured error matrix. The polishing process is performed by the Zeeko Company with an IRP600 machine. The Zeeko Company developed an innovative figuring and polishing approach, based on a patented tool (Bonnet tool) to provide a distributed pressure and variable area head for the polishing of aspheric and complex forms (Walker et al. 2002). It should be noted that a constant thickness polishing for surface damage removal is performed, before starting the correction process (moderation) to obtain the desired longitudinal profile, (Figure 2-2-B).

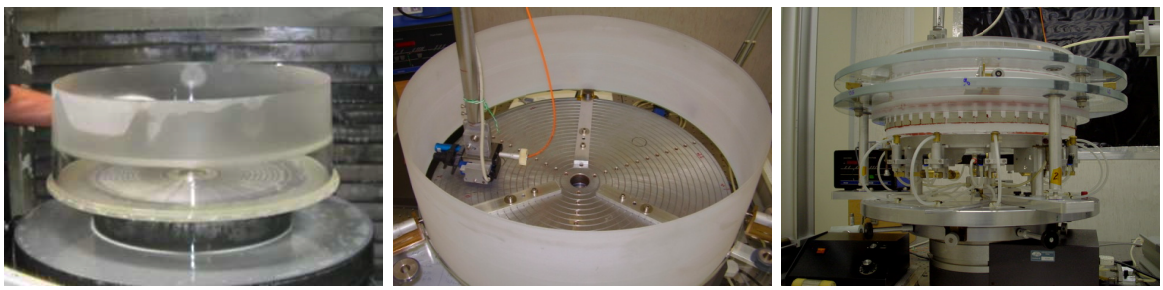

**(A)** **(B)** **(C)**

**Figure 2-1: The first part of the prototypal shell production flow: from raw fused silica tube to a double cone thin glass shell integrated in a temporary stiffening structure.**

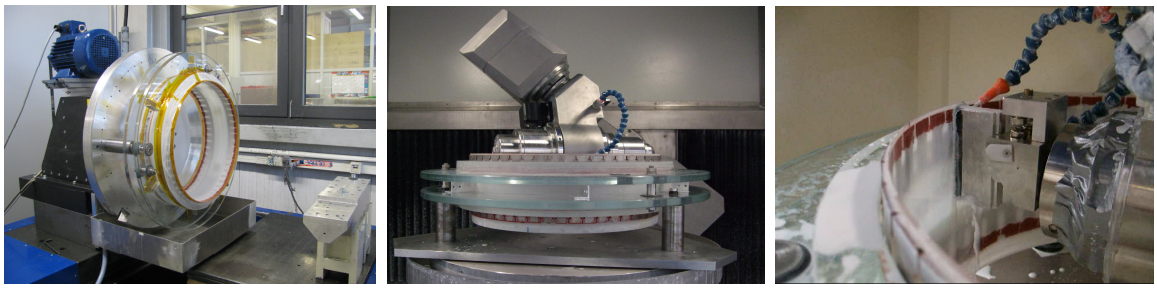

(A) (B) (C)

**Figure 2-2: The second part of the prototypal shell production flow: after the OOR correction on a precision diamond lathe with fine grinding, the optical surface quality is achieved trough deterministic polishing and the pitch super-polishing.**

- Once the desired profile is obtained by means of a proper moderation, a super-polishing process is finally performed by a suitable pitch tool mounted on the Zeeko CNC machine, in order to remove the remaining mid-frequency errors left by the Bonnet polishing (Figure 2-2-C).

The machining of the prototypal shell was stopped during the polishing work in November 2011 for a first X-ray verification at Panter facility (Figure 3-1). There was still an improvement to be done for what concerns the removal of errors with frequencies between 10 mm and 1 mm and to improve the micro-roughness. Nevertheless, measurements at Panter were important to compare the metrological results with the real X-ray results.

## 3. SHELL#7 X-RAYS MEASUREMENT RESULTS

The calibration of the shell has been performed at Panter facility, a 130 m long vacuum beam-line extensively employed for the test and calibration of X-ray optics and telescopes. The shell was mounted on a manipulator allowing the translation and the tilt ofteh shell for the alignment and best focus search. The last cleaning procedure on the shell and the shell mounted on the manipulator in the chamber are shown in Figure 3-2. We used two different detector setups:

- TRoPIC (Third Roentgen Panter Imaging Camera) detector: an energy sensitive CCD detector, with better than 0.2 keV energy resolution at low energies and 75 μm pixel size (corresponding to less than ~3" for our shell). The detector window side is 19.2 mm.
- PSPC (Position Sensitive Proportional Counter): a detector with spatial resolution of about 250 μm (10") and a field of view around 8 cm, used to make the raw alignment.

As the best focal plane of polynomial shell is curved, for each off-axis angle there is a best focus position that can be achieved adjusting the longitudinal position of the shell (around 5 mm in total). Due to the finite distance of the shell from the X-ray source, the focal plane is at 5200 mm instead of the theoretical one of 5000 mm. At the present stage the shell is not coated, nevertheless the reflectivity of the fused silica at an incidence angles of 0.7° is above 80% at 1 keV. X-ray measurements have been carried out in full illumination mode both with the PSPC and with the TRoPIC detector, on-axis and off-axis, in focus and out of focus and at different energies.

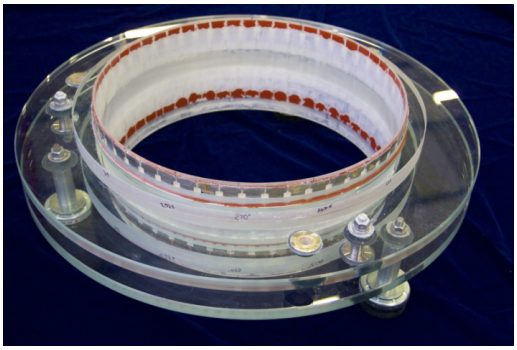

**Figure 3-1: The shell#7 within its support structure polished by Zeeko.**

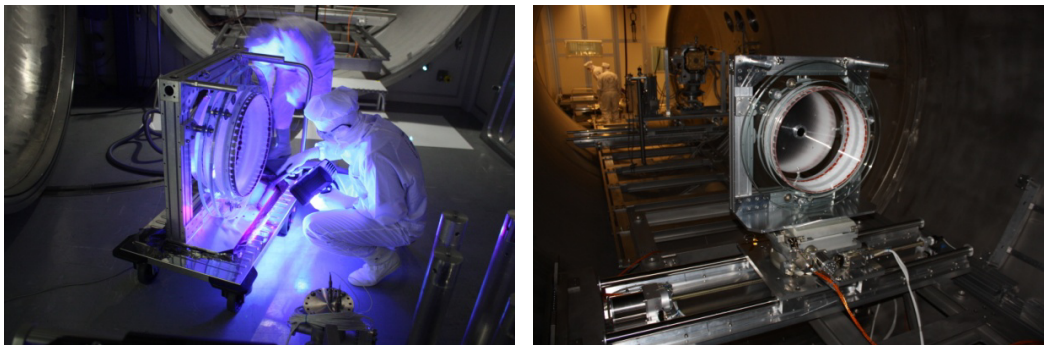

(A) (B)

**Figure 3-2: Two phases of the shell installation at the Panter facility.**

**On-Axis/off-axis shell measurement results.** One of the most important requirements of polynomial shells is a constant image quality across the field of view (FOV) in terms of Half Energy Width (HEW). As FOV is curved, the best position along the optical axis has been determined in order to carry out the measure. The best focus image acquired on axis and at 10', 20', 30' off-axis angles on the TRoPIC detector are reported in Figure 3-3. The results are presented with a pixel size equivalent to 25 μm at 0.93 keV, achieved with the sub-pixel resolution of MPE post-processing.

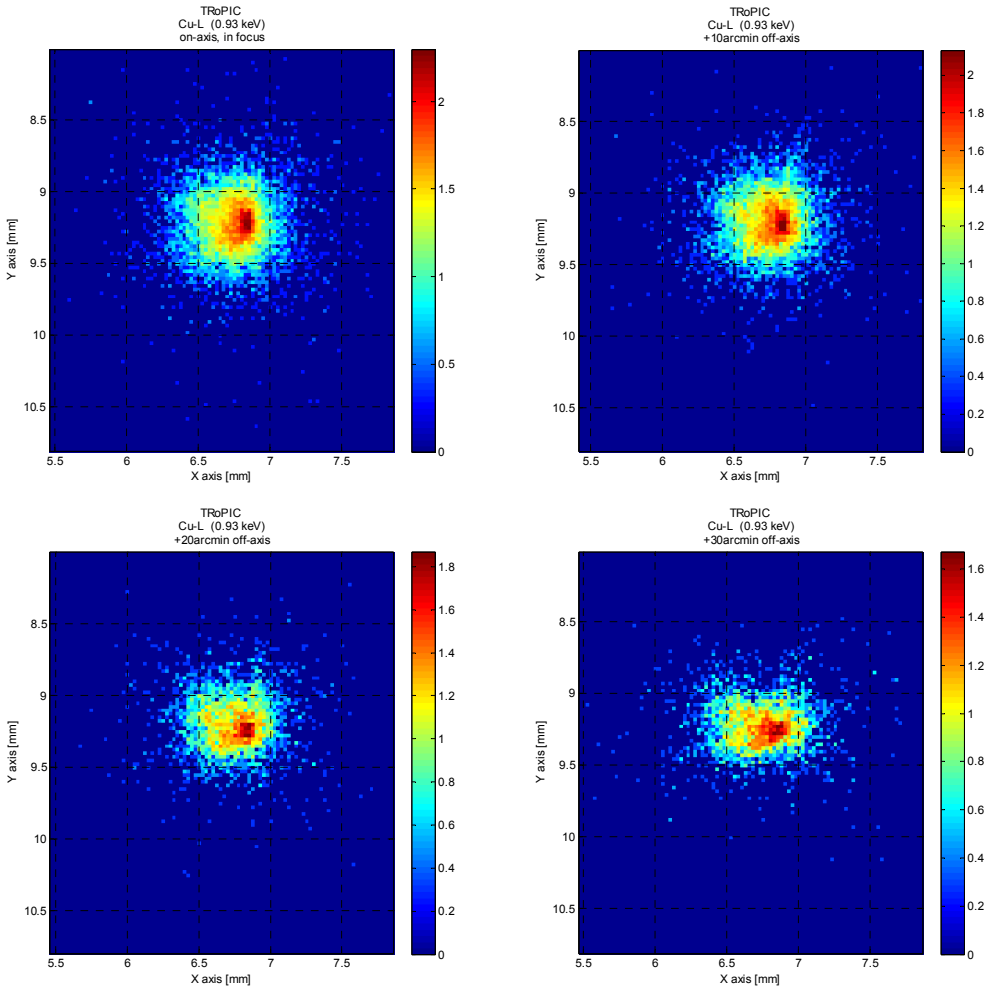


**Figure 3-3: Top Left, image at the best focal plane of a source on axis. Top right, the image at 10' off-axis. Bottom left, image at 20' off-axis. Bottom right, image at 30' off-axis.**

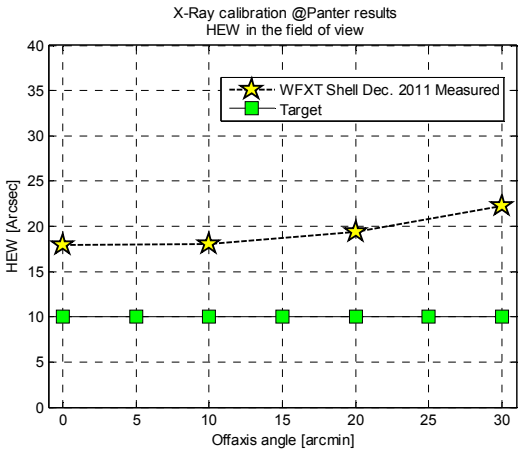


**Figure 3-4: HEW results as measured with TRoPIC at 0.93 keV as a function of the off-axis angle compared with our target.**

In Figure 3-4, the yellow stars indicate the HEW as measured at different positions of the field of view. As expected, the measured HEW is quite flat across the FOV. The values recorded varies from 17.8" on-axis up to 23.7" at 30 arcmin off-axis. It is important to stress that the polynomial design for the shell improves by a factor 4 the HEW with respect to a Wolter-I design of the same optical quality at the boundary of the field of view. As it can be noticed the HEW are larger than the specification values. We will now explain why, describing the correction action that must be taken to improve the image quality. It is evident that the on-axis image is not symmetric, with a halo on the left side. It has been demonstrated trough ray-tracing simulations that this result is compatible with a misalignment of the two optical axis of the front and rear segment of the shell. Therefore, after the X-ray calibration a measurement with a 3D CNC machine (UPMC) has been carried out on the shell. The measurements, taken at different heights on the shell, show that the (front and rear) optical axes were effectively misaligned by an angle of 4.8" (see left side of Figure 3-5). On a perfect shell, this kind of error causes a degradation of the HEW twice the value of the misalignment. The combination of this error with the others will be evaluated trough ray-tracing at the end of this paragraph where their estimation is provided. The result of a ray-tracing simulation taking into account the longitudinal profile errors, the measured OOR and the optical axis misalignment is reported on right side of Figure 3-5. The result is quite in agreement with the X-ray measurements and the combination of these errors degrades the expected HEW in the range of 18".

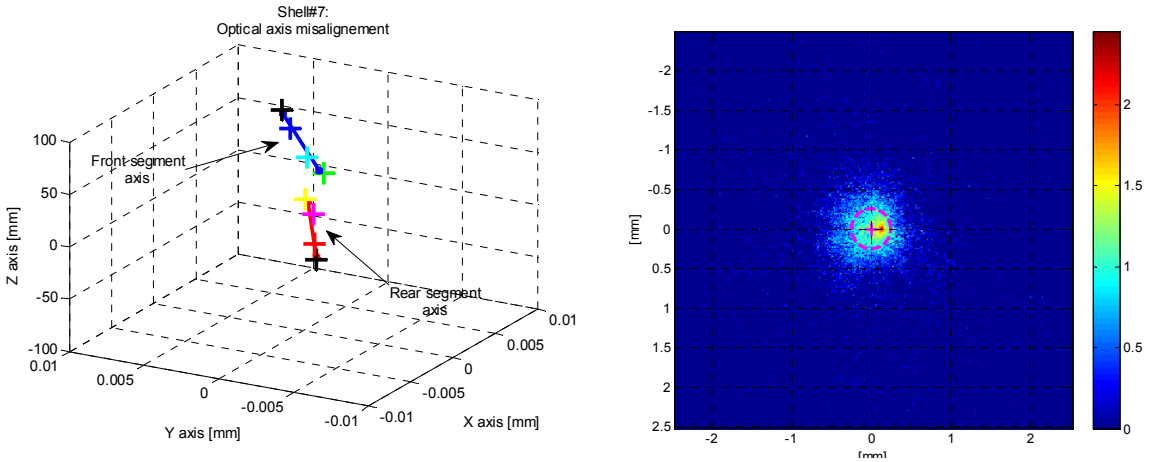


**(A)** **(B)**

**Figure 3-5: On the left optical axis determination trough measurement on UPMC. On the right, the ray-tracing simulation results taking into account the profile errors, the OOR and the optical misalignment.**

**On-Axis energy dependent shell measurement results.** Best focus on-axis images on the TRoPIC detector have been taken at different energies: 0.28 keV, 0.93 keV, 1.49 keV, 2.98 keV and 4.51 keV. The encircled energies at the different energies are shown in Figure 3-6. The measured HEW at different energies increases, as reported on the right panel in red. In this figure we compare the observed values with the calculated values assuming that the total HEW is the sum (quadratic in magenta or linear in cyan) of a constant term due to the figuring errors and of the scattering. The scattering contribution is calculated starting from the micro-roughness Power Spectral Density (PSD) (Spiga 2007). With this model, the contribution of the scattering is negligible at 0.93 keV. Therefore, all the errors contributing to the HEW should be due to geometrical shell error. The PSD model used for the calculation, reported on the left of Figure 3-7 in black, reproduces quite well the increase of the HEW. In the same figure we show the PSD as determined from the AFM measurements (on 100 µm and 10 µm scale) and PGI measurements on the profiles at the four azimuth directions of the shell (0°, 90°, 180° and 270°). As expected, the AFM measurements show that we have not reached the micro-roughness requirements; while the PGI measurements show that features on the scale of ~125 µm have still to be removed.

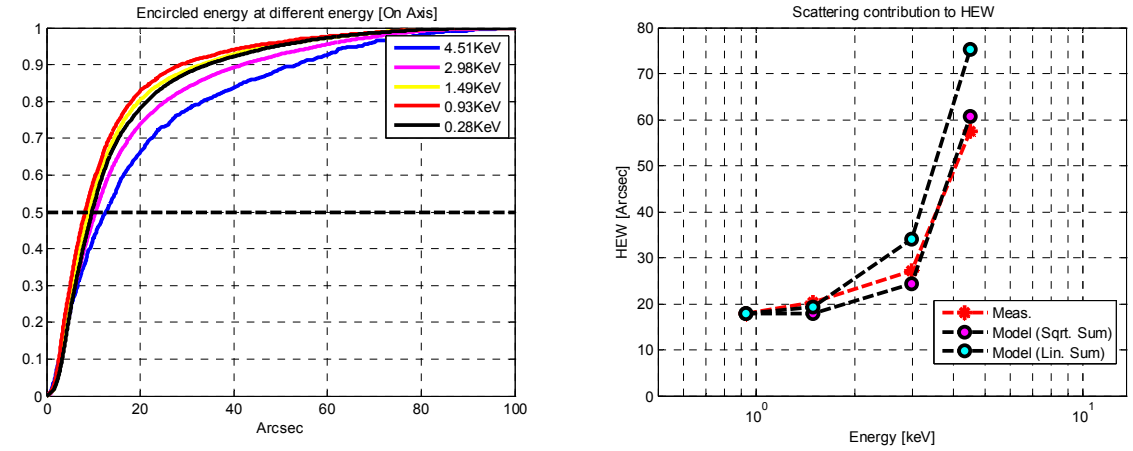


**(A)** **(B)**

**Figure 3-6: Panel A shows the encircled energies as measured at 0.28 keV, 0.93 keV, 1.49 keV, 2.98 keV and 4.51 keV. Panel B reports the dependence of the measured HEW on the energy: in red the HEW values as measured taking into account the TRoPIC detector. Cyan and magenta points are the expected values inferred from the scattering model with to the PSD plotted in black in Figure 3-7.**

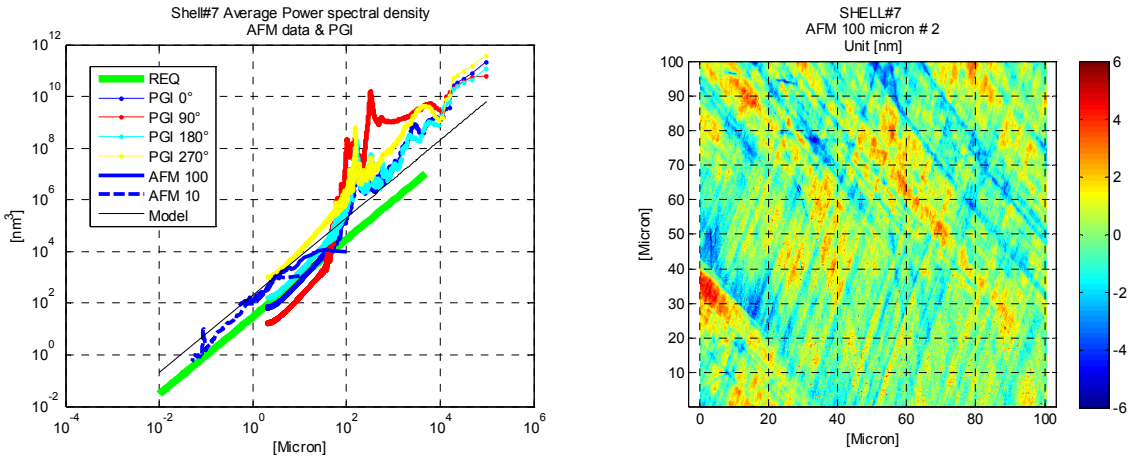


**(A)** **(B)**

**Figure 3-7: In panel A, the PSD of the longitudinal profile data (colored lines) and the PSD from the AFM data (100 µm and 10 µm). In panel B, a map of AFM on 100 µm scale.**

Table 3-1: Measured micro-roughness values compared with the required values.

| Instrument | Frequency range | Sigma Req. Value | Sigma Meas. Value |
|---|---|---|---|
| AFM 10 | 0.05 μm - 5 μm | 3.5 Å | 7 Å |
| AFM 100 | 0.5 μm - 50 μm | 5.0 Å | 12 Å |

The right panel of Figure 3-7 shows an image as taken on 100 μm scale with the AFM. Table 3-1 reports the values of σ for both the measurements and the requirement values at that scale. When we interrupted the super-polishing activities, in order to perform the intermediate X-ray calibrations, we were at twice the value of the specification.

**Out-of-focus shell measurement results.** In order to evaluate the contribution of the out-of-roundness, we have measured the annular ring of the shell at intra-focal and extra-focal distance with respect to the best focus. The results obtained with PSPC are reported in Figure 3-8. The measurements performed with the TRoPIC detector are reported in Figure 3-9. While the measures with the PSPC have been carried out at ±200 mm distance from the shell best focus, the measures with TRoPIC have been carried out at ±125 mm and ±35 mm from the best focus.
All the measurements confirm that the OOR of the shell is quite good, while the roughness changes azimuthally. From the TRoPIC measurements, the different smearing of the photons due to roughness is visible for different azimuth directions. This is in line with the fact that the reflectivity of a surface decreases for higher value of the roughness, as the missing photons correspond to the scattered component. At the moment we do not have a complete characterization of the shell roughness in terms of bandwidth and positions.

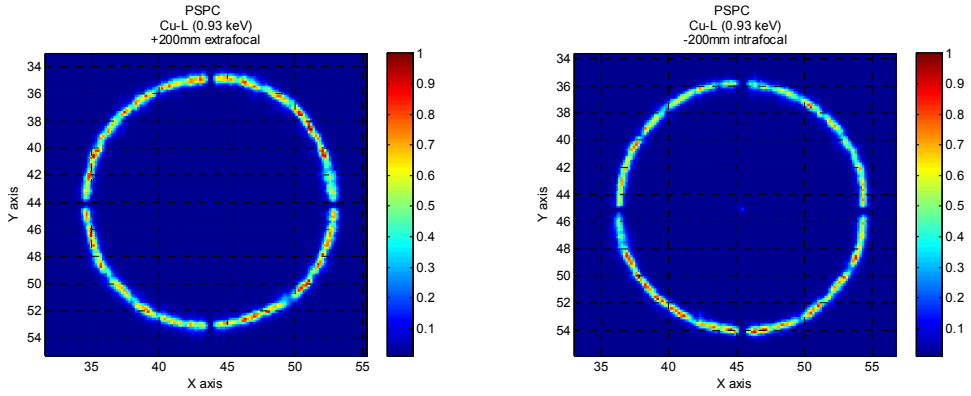


**(A)** **(B)**

**Figure 3-8: Extra-focal and intra-focal shell annular ring as measured with PSPC. Color scale is normalized to the pixel with the maximum number of counts.**

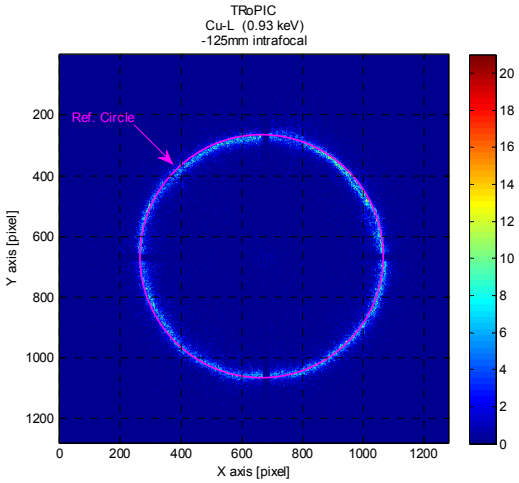


**Figure 3-9: Intra-focal annular ring as measured with TRoPIC. Color scale is reporting the number of event recorder for pixel. In pink a perfect reference circle for comparison.**

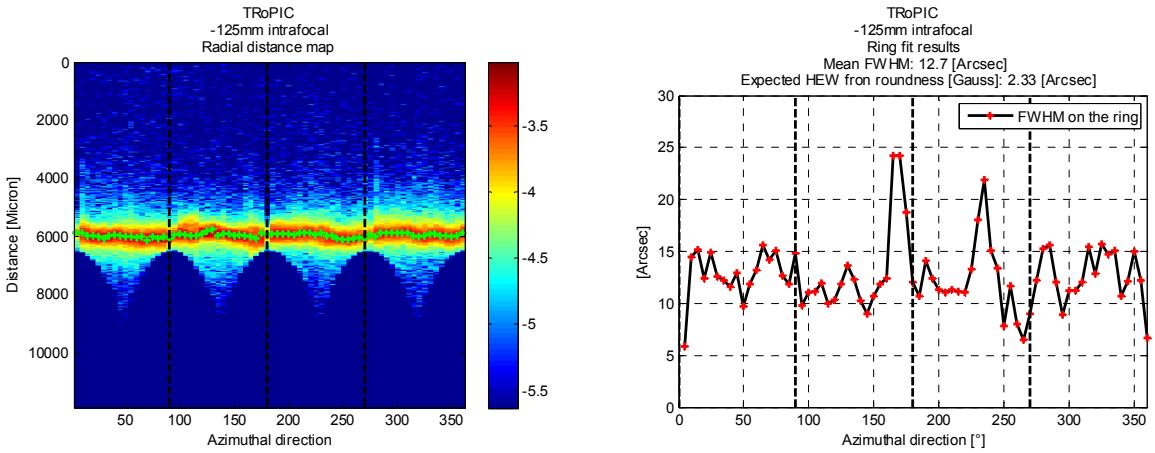


**(A)** **(B)**

**Figure 3-10: On the left, photon distribution on radial beams: the red crosses are the point where the maximum of Gaussian fits are found. Their displacements can be related to the longitudinal profile error and/or to the OOR of the shell. Their contributions in terms of HEW is of around 2". On the right, the FWHM as calculated on the radial profiles. The mean value is around 13", while in a segment of the shell it reaches more than 20".**

The detailed micro-roughness characterization needed to make an assessment on the polishing results has not been completed, yet. This because the measurement set-up is complicated by the vibrations of the monolithic shell. Figure 3-9 shows as an example the ring measured at 125 mm intra-focal with the TRoPIC, compared with a theoretical reference circle. By integrating the photons distribution on radial beams, we can recover the radial profiles of their distribution along the different azimuth. The result obtained is reported in the left panel of Figure 3-10. In a theoretical model the radius of the maximum of the radial profiles should be constant for all the azimuthal directions. Deviation from this reference position may be due to the OOR errors or to slightly different focal length of the profiles. We can estimate the impact on the combination of these errors from the misplacement of the radial position of the peaks of the radial profile Gaussian fit. For the HEW the contribution is around 2". The right panel of Figure 3-10 shows the variation of the FWHM of the radial profiles as a function of the azimuth. Data have been integrated in beams of 5°. The mean value is around 13", while in a segment of the shell it is more than 20": this reflects the differences in the micro-roughness achieved in different sectors.

**Intermediate calibration conclusions.** The analysis of the X-ray calibration data and the comparison with the available metrological data shows that these results can be explained in agreement with the partition reported in Table 3-2. The low frequency longitudinal profile errors (as derived from the PGI measurements) contribute 6" to the final angular resolution on the on-axis data at 0.93 keV. Adding OOR (as derived from OAB roundness meter) to the ray-tracing simulations, increases the value to 8". Adding to the simulations the degradation introduced by the optical axis tilt, rises the expected result to 12". Finally, considering also the longitudinal profile mid-frequencies contribution, we derive an expected HEW of 17". This error decoupling analysis indicates that the micro-roughness and the mid-frequencies profile errors have still to be improved in order to reach an HEW below 10", but we were on the right track. What was not expected, is the error on the optical axis alignment that can prevent us to reach the 10" HEW goal, even after the mid-frequencies error are corrected. Unfortunately, the shell has been damaged during the post-calibration measurement activities and the programmed final polishing on this shell could not be carried out. This aspect will be monitored and prevented during the manufacturing of the shell#8.

**Table 3-2: Decoupling error table.**

| Long. Low Freq. errors | OOR | Opt. axis relative tilt | Long. Mid Freq. errors | 0.93 keV RT inferred HEW |
|---|---|---|---|---|
| x | | | | 6" |
| x | x | | | 8" |
| x | x | x | | 12" |
| x | x | x | x | 17" |

## 4. FURTHER INVESTIGATION ON SHELL#8

Due to the damage of shell#7, a new shell with the same geometry has been integrated in a SSS and will go through the fine grinding. Considering that the processing of the shell will be done with the optical axis in horizontal and in vertical positions, a number of measurements have been carried out on this new shell. The aim is to characterize as much as possible the behavior of the shell in the various mounting steps that have to be managed during the process and for the final measure with X-ray at Panter. The scope is to determine if there could be possible improvements in the mounting concept, in particular for the next calibration. When the shell is integrated in the SSS it has to be sustained with the optical axis orthogonal to the gravity. It is supported trough three spacers that interface the late or the jig for calibration at Panter. This jig, called hereafter Panter jig, is made of aluminum and is basically a reference square with three fixing points separated by 120°, one on the bottom and two at the top.

As the new shell is not yet machined, its initial OOR are quite high with respect to the final required values, to be achieved with the fine grinding and the polishing. Therefore, we focused on the possible OOR error variations due to the different mounting. The measured values and their variations can be considered upper limit with respect to the deformation expected on the final shell. Different kind of analyses have been carried out using, when possible, the roundness meter available at OAB and the metrology facility of Zeiss in Novara (Italy), where a 3D machine with an accuracy of 1.5 micron is available. We have analyzed how the shell shape changes when it is integrated on the Panter jig and when the shell is sustained with the optical axis parallel or orthogonal to gravity. Moreover, we evaluated if there are modifications in the shell shape when it is kept for several days with the optical axis orthogonal to gravity, due to possible glue creep effects. These information are important to define if the SSS is a fully suitable device to guarantee the optimal sustain of the shell both when it is with the optical axis directed as gravity or transversal to it. In Figure 4-1 we report the measurement schemes. Assuming the reference configuration with the shell integrated in the SSS and measured on the roundness meter with the optical axis aligned with the gravity one (panel A), the measure is repeated in the same configuration but with the shell integrated in the Panter jig (panel B) to determine if the integration into the jig causes deformations. Then taking this new measure as a new reference, the shell in the SSS with the supporting jig is rotated by 90° in the reference configuration assumed during the X-ray calibration (Panel C). The last comparison regards the measure in this configuration and the repeated one a few days later.

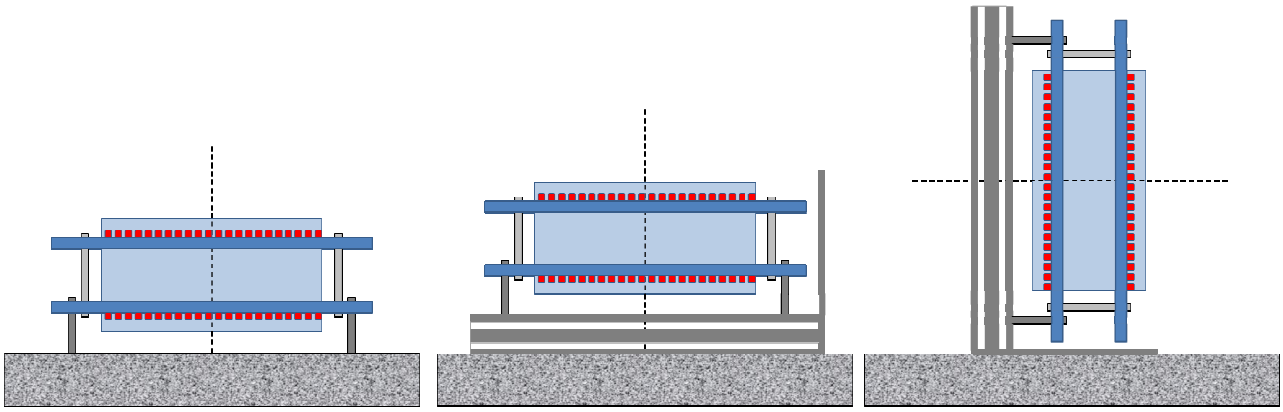


**Figure 4-1: The three mounting set-up to be compared: the reference configuration with the shell integrated in the SSS and measured on the roundness meter with the optical axis aligned as the gravity (panel A). The shell in the SSS is integrated in the Panter jig (panel B). The shell in the SSS with the supporting jig is rotated by 90° in the reference configuration used during the X-ray calibrations (Panel C).**

**Deformation caused by the Panter jig through OOR measurements on roundness meter.** The comparison of the measurement on the roundness meter with the shell on the SSS or integrated in the Panter jig, has been carried out after the measurement at Zeiss with the 3D CNC machine. During these measurements it was found that the OOR on the Phi_min side (rear side) were higher than expected: they were not in line with the ones achieved with the shell in the SSS but without the Panter jig. After the confirmation that dismounting the shell the OOR measurements return back to previous values, the shell has been remounted several times to see how much the error was repeatable. In Figure 4-2 we show the OOR values as acquired on the roundness meter with the shell in condition A and B, respectively. The height

of the measure indicates the distance from Phi_max (front side). The measures have been taken starting from 5 mm from the top edge of the shell and with steps of 10 mm. The OOR of the shell integrated in the SSS are reported on the left panel. Peak-to-Valley (PtV) values are of the order of 15 µm on the edge of the shell. The rear surface shows a tri-lobe shape while on the front surface of the shell the ovalization is the major contribution. From these OOR measurements, the optical axis of the two surfaces (front and rear) and their relative alignment has been extrapolated removing the same first decentering component from each OOR acquired data. The inferred misalignment is around 3.4" and the decentering is of the order of 2 µm. On the right panel of Figure 4-2 we plot the OOR of the shell in the SSS mounted on the Panter jig (configuration B). OOR PtV values are larger and the shape of the OOR changed significantly on Phi_min. The integration process has been repeated several times in order to verify its repeatability. In Figure 4-3 we report the results in terms of the OOR PtV. The shape of the OOR errors changes significantly with the integration in the Panter jig. Larger differences are evidenced on Phi_min, that is where the SSS is connected to the Panter jig. The OOR variations can be of the order of 35 µm PtV. The directions of the errors are in good agreement. In Figure 4-4 we show as an example the OOR as measured on Phi_max and on Phi_min during different repeated mountings. The black line reports the original OOR shape.

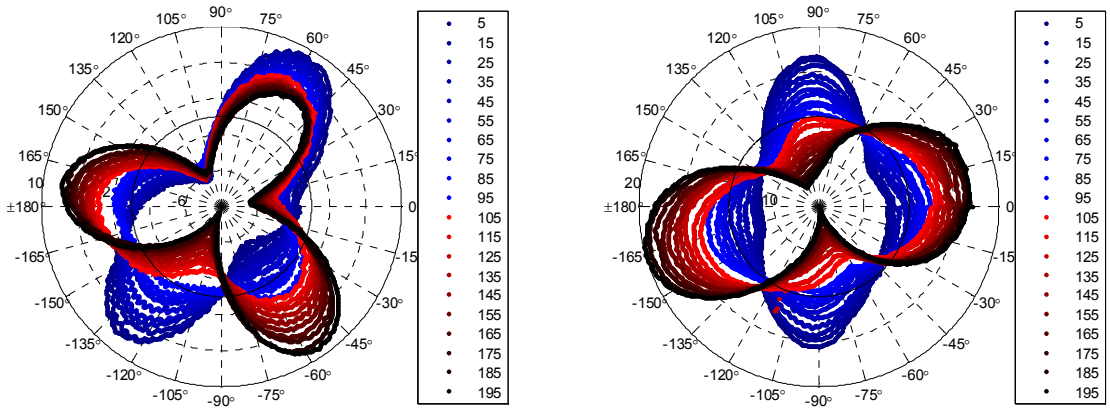


**(A)** **(B)**

**Figure 4-2: measured OOR for the shell#8: on the left the shell is integrated in the SSS. On the right, the shell with the SSS is mounted on the Panter jig. Measures are not aligned on the same 0 reference point.**

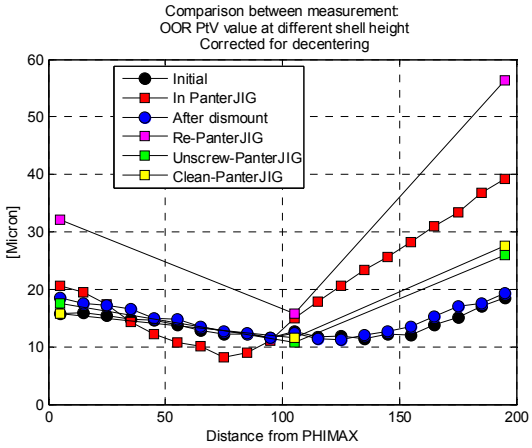


**Figure 4-3: PtV OOR along the optical axis measured on the shell in several repeated configurations.**

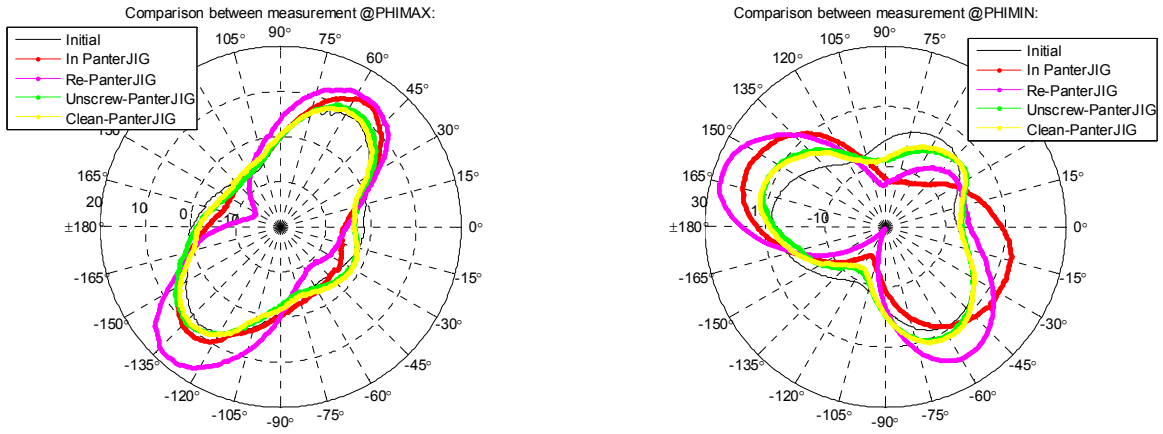


**(A)** **(B)**

**Figure 4-4: The OOR as measured on Phi_max and on Phi_min. In black the initial measurements, in red the measure in the Panter jig, in magenta after the re-mount, in green with the shell in the SSS placed over the jig without fixing it, in yellow after the cleaning of the interfaces and correct centering.**

The OOR data as acquired in the different configurations have been used in the ray-tracing simulations to evaluate the contribution of the deformations induced by the mounting on the Panter jig. The maximum variability in terms of HEW is 5". Therefore, it is necessary to review the design of the Panter jig. This result indicates that part of the HEW of shell#7, measured during the X-ray calibration, is probably due to this effect.

**Horizontal vs. vertical configuration by 3D measurements.** This measurement campaign has been carried out at Zeiss (Novara, Italy) with shell#8 integrated on a SSS. Given that the shell shape has not yet been corrected trough fine grinding, the OOR values are of the order of 15-20 μm at Phi_max and Phi_min and around 10 μm at the intersection plane.

In order to perform the measurements with the optical axis of the shell placed both in horizontal and in vertical conditions, the shell in the SSS was mounted on the same jig used to test shell#7 at Panter. In Figure 4-5 we report two images of the measurement configurations. In the first, the shell is with the optical axis aligned with gravity. In the second, the shell is with the optical axis orthogonal to gravity. On the left panel of Figure 4-6 are reported the PtV of the OOR at different height of the shell. In red are the values corresponding to the shell with the optical axis parallel to gravity while blue and cyan values correspond to the configuration with the optical axis orthogonal to gravity, during consecutive measurements. Note that while the repeatability of consecutive measurements is below 1 μm, measurements performed after a repositioning of the shell show differences with PtV of the order of 2 μm. In green are shown the PtV OOR of the shell as measured after 5 days of permanence in the condition with the optical axis orthogonal to gravity. The measured effects are within the measurement errors.

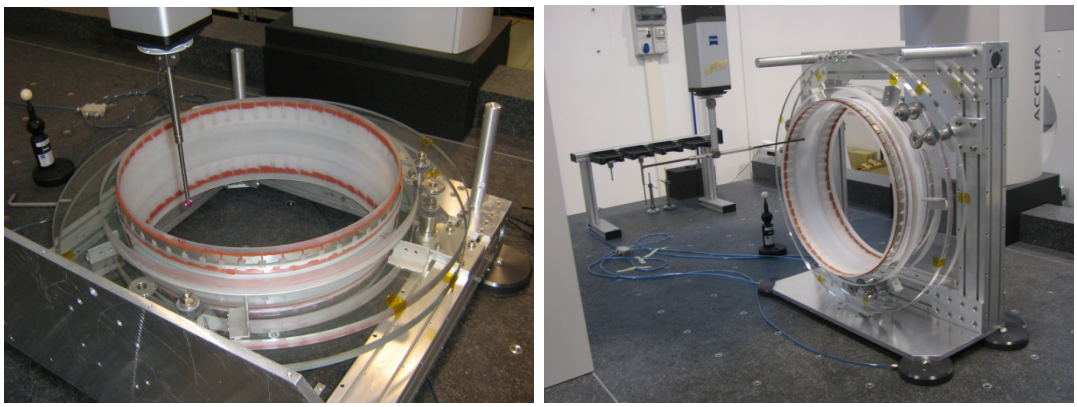


**Figure 4-5: The measurement configuration of the shell with the optical axis aligned with the gravity and with the optical axis orthogonal to gravity (Panter configuration).**

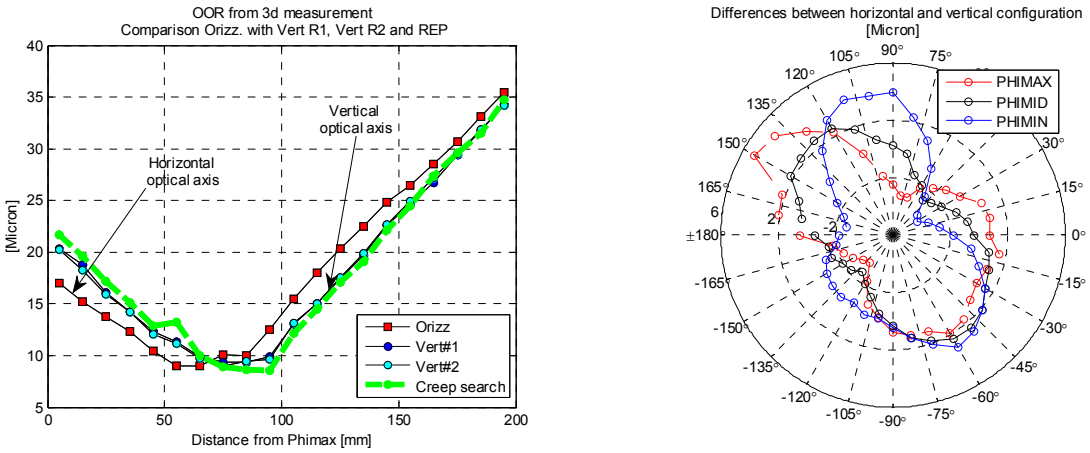


**Figure 4-6: On the left, the PtV of the OOR as measured with the shell with the optical axis parallel (Vert#1 and Vert#2) and orthogonal to gravity (Orizz). On the right, colored circles indicate the subtraction of the measured OOR curves as measured in vertical and in horizontal at different shell heights.**

On the right panel of Figure 4-6, colored circles show the differences between the two measurements with the optical axis horizontal and vertical. The differences are of the order of 8 μm PtV and their impact on the HEW is around 4". Because finite elements simulations indicate that the differences between vertical and horizontal configurations should not be greater than 1", we infer that the observed changes are related to the stiffness of the Panter jig.
According to the results presented, the design of the Panter jig has to be modified improving its stiffness in order not to deform the shell in all the configurations.

## 5. CONCLUSIONS

The realization of a prototypal shell made of thin glass with polynomial design has been carried out through all the foreseen steps up to intermediate X-ray calibration tests in December 2011 at Panter. The measured HEW of the shell is below 20" for almost all the field of view and the results are in line with expectations based on metrology. The results are quite promising as the completion of the super-polishing activities and the removal of the optical axis misalignment tilt would allow us toreach the goal of HEW≤10" over the ful FOV of 1 degree.
As the prototypal shell#7 has been broken during a metrology campaign, the development of a new shell is in progress: all the improvements found during the processing of shell#7 will be implemented in the machining of the new one. The new shell (shell#8) is already integrated in the SSS and is ready for the starting of fine grinding activities with the diamond late. This operation will be executed with a succession of grinding wheel with decreasing grain size (30-20-5 μm). In this way a lower Sub-Surface-Damage is expected with respect to the one obtained on shell#7, where only grain size of 30 μm were used. This is expected to reduce the amount of material to be removed during the polishing phase and therefore the global machining time that will be monitored with particular care in order to determine the time necessary for the realization of a complete optical system.

## ACKNOWLEDGENTS

This work is supported by ASI and INAF grants. We are grateful to the WFXT collaboration and, in particular, to S. Murray and R. Giacconi, for supporting this work and many useful discussions. We acknowledge Heraeus Quarzglas GmbH & Co KG for the manufacturing of the raw glass shells.

## REFERENCES

[1] S. S Murray, et al., 'Wide Field X-Ray Telescope Mission', A white paper submitted in Response to Solicitation NNH11ZDA018L.
[2] P. Conconi, G. Pareschi, S. Campana. O. Citterio, M. M. Civitani, V. Cotroneo, L. Proserpio, G. Tagliaferri, G.

Parodi, Proc. SPIE, 7437, 74370D-1 (2009).
[3] C. J. Burrows, R. Burg, R. Giacconi, ApJ, 392, 760 (1992).
[4] P. Conconi, S. Campana, G. Tagliaferri, G. Pareschi, O. Citterio, V. Cotroneo, L. Proserpio, M. M. Civitani, MNRAS, 405, 877 (2010).
[5] P. Conconi, S. Campana, A&A, 372, 1088 (2001).
[6] O. Citterio, M. M. Civitani, J. Arnold, S. Campana, H. Combrinck, P. Conconi, V. Cotroneo, R. Freeman, E. Mattaini, R. Morton, G. Motta, G. Pareschi, G. Parodi, L. Proserpio, S. Schuler, P. Simpson, G. Tagliaferri, D. Walker, Proc. SPIE 8147, 8147-14 (2011).
[7] D. Spiga, A&A 468, 775 (2007).
[8] D. D. Walker, A. T. H. Beaucamp, D. Brooks, R. Freeman, A. King, G. McCavana, R. Morton, D. Riley, J. Simms, Proc. SPIE, 4451, 267 (2002).